DALTON
FULL PAPER

Molecular modelling studies of N-salicylideneamino acidato complexes of oxovanadium(IV). Molecular and crystal structure of a new dinuclear $LOV^{IV}–O–V^{V}OL$ mixed valence complex †‡

João Costa Pessoa,*[a] Maria J. Calhorda,[b,c] Isabel Cavaco,[a,d] Isabel Correia,[a] M. Teresa Duarte,[a] Vitor Felix,[f] R.T. Henriques,[a,e] Maria F. M. Piedade[a,c] and Isabel Tomaz[a]

[a] *Centro Química Estrutural, Instituto Superior Técnico, Av. Rovisco Pais, 1049-001 Lisboa, Portugal*
[b] *Instituto de Tecnogia Química e Biológica, Av. da República, Apt. 127, 2781-901 Oeiras, Portugal*
[c] *Departamento de Química e Bioquímica, Universidade de Lisboa, Campo Grande, 1744-016 Lisboa, Portugal*
[d] *Now at Universidade do Algarve, Unidade de Ciências Exactas, Campus de Gambelas, 8000 Faro, Portugal*
[e] *Instituto Tecnológico e Nuclear, Departamento de Química, Estrada Nacional 10, 2685- Sacavém, Portugal*
[f] *Departamento de Química, Universidade de Aveiro, 3810-193 Aveiro, Portugal*

Received 7th July 2002, Accepted 24th September 2002
First published as an Advance Article on the web 28th October 2002

The dinuclear complex $Na[V_2O_3(MeOsal\text{-}L\text{-}Ile)_2]\cdot H_2O$ **1** (MeOsal-L-Ile = 4-methoxysalicylidene-L-isoleucinate) has been prepared and characterised and its crystal structure determined. The molecule consists of two *C*-VO(MeOsal-L-Ile) units, the Schiff base ligand being approximately planar. Each unit exhibits a distorted square-pyramidal coordination geometry around the V atoms involving the O,N,O atoms of the Schiff base ligand and the bridging O(oxo) atom. The $V^{IV}–O–V^{V}$ bridge is almost linear (angle: 170.9(3)°), indicating extensive electron delocalization, and the V–O(oxo) bond lengths are 1.811(5) and 1.836(5) Å. Molecular mechanics (MM) and density functional theory (DFT) methods are used to calculate the structures and the main factors that determine the relative energies of the *CL*- and *AL*-$[V^{IV}O(sal\text{-}aa)(X)]$ diastereomeric complexes (aa = N-salicylidene-amino acidate, X = H_2O or 2,2′-bipyridine). The results obtained indicate that for X = bpy the *CL*-diastereomers are more stable than the *AL*-diastereomers, and the energy differences increase with the degree of substitution on the β-carbon atom of the amino acid. For X = H_2O the *CL*- and *AL*-diastereomers correspond to about the same energies. DFT methods are also used to calculate the IR spectrum of *C*-$[V^{IV}O(sal\text{-}L\text{-}Ala)(H_2O)]$ (sal-L-Ala = N-salicylidene-alaninate) which compares well with the experimental, and the g_x, g_y, g_z, and A_x, A_y, A_z parameters of the EPR spectra. The structure of $[V_2O_3(HOsal\text{-}L\text{-}Gly)_2]^-$ was also calculated by DFT methods and compared with the X-ray structure of **1**.

Introduction

Schiff bases (SB) derived from the reaction of aromatic aldehydes and amino acids have been the subject of extensive research, typified by their vanadium compounds.[1–26] With vanadium-(IV) and -(V) these SB complexes often have coordination geometries such as those in **I** or **II**.[2,5,15] In a few cases, dinuclear oxo-bridged $V^{IV}–O–V^{V}$ or $V^{V}–O–V^{V}$ compounds **III** have been obtained[2,7,14,16,24] and were characterised by X-ray diffraction.

Upon standing in methanolic solution in air $[V^{IV}O(sal\text{-}aa)(H_2O)]$ complexes (sal-aa = N-salicylideneamino acidate) are spontaneously oxidised to $[V^{V}O(sal\text{-}aa)(OMe)(OHMe)]$ **II**.[1,2,11,14,16] In some systems, dinuclear compounds **III** have been obtained and we report one such case in the present study: $Na[V_2O_3(MeOsal\text{-}L\text{-}Ile)_2]\cdot H_2O$ **1** (MeOsal-L-Ile = 4-methoxysalicylidene-L-isoleucinate). If 2,2′-bipyridine (bpy) or pyridine (py) is present in solution, it coordinates to $V^{IV}O^{2+}$ forming complexes such as **IV**, and oxidation may be slowed down or avoided.[1,9,11,15]

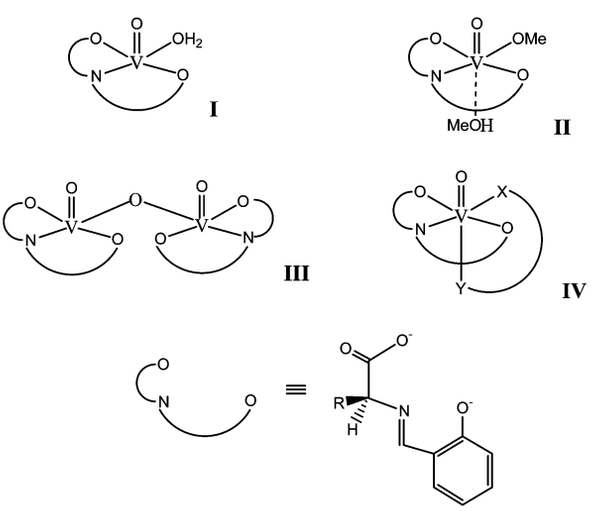

I **II** **III** **IV**

As emphasised previously,[9,12–18,23,27] apart from the chirality of the amino acid moiety, two enantiomers **Va** and **Vb** may be considered for each Schiff base complex. This is a general characteristic of vanadyl complexes of this type, *i.e.* those with at least two non-equal adjacent equatorial donor atoms in a

† Electronic supplementary information (ESI) available: theoretical background and additional data. See http://www.rsc.org/suppdata/dt/b2/b205843j/
‡ Non-SI units employed: 1 kcal = 4.184×10^3 J.

Table 1 Vanadium Schiff base complexes derived from the reaction of *o*-hydroxyaromatic aldehydes with amino acids (mostly characterised by X-ray diffraction). Summary of the relative position of the V=O and amino acid side groups

Complex [a]	Configurations [28] of the amino acid and metal centre in the solid state [b,c]	Comments [d]
$[V^{IV}O(sal\text{-}L\text{-}Ala)(H_2O)]$ [5]	*CL* (*endo*)	
$[V^{IV}O(sal\text{-}D,L\text{-}Asn)(py)(H_2O)]$ [15]	*CL* (*endo*), *AD* (*endo*)	
$[V^{IV}O(sal\text{-}L\text{-}Ala)(bpy)]$ [9]	50% *CL* (*endo*) + 50% *AL* (*exo*)	
$[V^{IV}O(pyr\text{-}D,L\text{-}Ile)(bpy)]$ [23]	*CL* (*endo*), *AD* (*endo*)	
$[V^{V}O(sal\text{-}L\text{-}Ala)(OCH_3)(HOCH_3)]$ [2]	*CL* (*endo*)	Solution ^{1}H NMR: relative proportion of diastereomers = 3:4
$[V^{V}O(sal\text{-}L\text{-}Val)(OCH_3)(HOCH_3)]$ [20]	*CL* (*endo*)	
$[V^{V}O(sal\text{-}L\text{-}Phe)(hquin)]$ [12]	*CL* (*endo*)	Solution ^{1}H NMR: no evidence for the presence of any *AL*-diastereomer
$[V^{V}O(sal\text{-}L\text{-}aa)(Hpd)]$ [18]	—	Solution ^{51}V NMR: K = 1.7 (Ala), 10.7 (Val); 2.1 (Phe)
$[V^{V}O(sal\text{-}L\text{-}aa)(Hpt)]$ [18]	—	Solution ^{51}V NMR: K = 6.2 (Ala), 40.0 (Val); 8.3 (Phe)
$[V^{V}O(sal\text{-}L\text{-}Phe)(MP)]$ [19]	*CL* (*endo*)	Solution ^{51}V and ^{1}H NMR: only *endo* isomer detected
$[V^{V}O(sal\text{-}L\text{-}Ala)(pbh)]$ [21]	50% *CL* (*endo*) + 50% *AL* (*exo*)	
$[V^{V}O(sal\text{-}L\text{-}Phe)(Hed)]$ [26]	*CL* (*endo*)	Solution ^{1}H NMR: *AL*-diastereomer not detected
$Et_4N[V^{IV}V^{V}O_3(sal\text{-}L\text{-}Ala)_2]$ [16]	*CL* (*endo*)	
$Na[V^{IV}V^{V}O_3(sal\text{-}D,L\text{-}Ser)_2]$ [7]	*CL* (*endo*), *AD* (*endo*)	
$[V^{V}_2O_3(sal\text{-}L\text{-}Val)_2(H_2O)]$ [14]	*CL* (*endo*)	
$[V^{V}_2O_3(van\text{-}L\text{-}Ser)_2(H_2O)]$ [24]	50% *CL* (*endo*) + 50% *AL* (*exo*)	
$Na[V^{IV}V^{V}O_3(sal\text{-}L\text{-}Ile)_2]$ [e]	*CL* (*endo*)	
$[V^{V}O(naph\text{-}L\text{-}Ala)(OBu^s)(HOBu^s)]$ [13]	50% *CL* (*endo*) + 50% *AL* (*exo*)	Solution ^{51}V NMR: at least 3 diastereomers in solution
$[V^{V}O_2(naph\text{-}His)]$ [8]	*CL* (*endo*)	

[a] The Table includes all reported vanadium complexes characterized by X-ray diffraction with the sal-aa ligands, but not all reported structures with other similar Schiff base ligands. [b] For isomers *CL*, the relative position of the V=O and side groups is *endo*; for *AL* it is *exo*. This is valid for [VO(sal-L-aa)(H_2O)] complexes. For several of the six-coordinate compounds considered, where one H_2O ligand is substituted by a different donor atom, the priority rules[28] may yield a different configuration at the metal centre. However we use the same *C* or *A* notations for identical disposition of the O, N, O donor atoms of the SB ligand in relation to the V=O group. [c] Hhquin = quinolin-8-ol; bpy = 2,2′-bipyridine; H_2ed = $HO(CH_2)_2OH$; H_2pd = $HO(CH_2)_3OH$; H_2pt = $HOCH(CH_2OH)CH_2OH$; GP = methyl-2,6-dimethoxy-β-D-galactopyranoside; pbh = *N*-phenylbenzohydroxamato-*O*,*O*′; MP = methyl-4,6-dimethoxy-α-D-mannopyranoside; $HOBu^s$ = D,L-*sec*-butyl alcohol; van = *o*-vanillin; naph- = naphthalidene (*N*-(2-oxido-1-naphthylmethylene-). [d] $K = [CL]/[AL]$ ([*CL*]: concentration of the *CL*-diastereomer, [*AL*]: concentration of the *AL*-diastereomer. [e] This work.

chelate molecule.[27] When the Cα methylene group is substituted to form –CHR, two diasteromeric pairs of isomers may form: for an L-amino acid: *CL*- (≡ **Va** – *endo*) and *AL*- (≡ **Vb** – *exo*); for a D-amino acid: *CD*- and *AD*-, giving a total of four.[28] In almost all monomeric $[V^{IV}O(sal\text{-}aa)(X)]$ (**I**, **II** and **IV**) and dinuclear **III** complexes (aa = amino acid, X = H_2O, py, bpy, hquin, or other ligands; Hhquin = 8-quinolinol) characterised by X-ray diffraction, only the *endo* isomers have been obtained (Table 1). The only exceptions are $[V^{IV}O(sal\text{-}L\text{-}Ala)(bpy)]$[9] and $[V^{V}O(sal\text{-}L\text{-}Ala)(pbh)]$ (pbh = *N*-phenylbenzohydroxamate).[26]

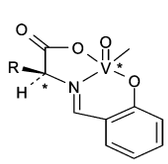

Va: (*CL*→*endo*)

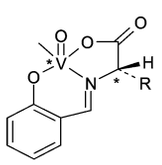

Vb: (*AL*→*exo*)

In $[V^{IV}O(sal\text{-}aa)(H_2O)]$ and $[V^{IV}O(sal\text{-}aa)(bpy)]$ complexes, this type of diastereoisomerism has been suggested as an explanation for the increase in the Cotton effect in the visible range as the bulkiness of the amino acid side-group increases.[14] In $[V^{V}O(sal\text{-}aa)(diol)]$ complexes, the presence of two ^{51}V NMR signals has been ascribed to the equilibrium between diastereomers **Va** and **Vb**, and from certain signals of the ^{1}H NMR and ^{51}V NMR spectra the equilibrium constants K = **[Va]**/**[Vb]** were found to be between 2 and 40 (Table 1), depending on the size of the diol chelate ring and on the bulkiness of the R side-group.

Molecular mechanics (MM) has been occasionally applied to oxovanadium complexes[29,30] namely for $[V^{V}O(sal\text{-}L\text{-}Ala)(OCH_3)(CH_3OH)]$.[30] A near degeneracy of isomers **Va** and **Vb** was found (**Va** more stable by 0.1 kcal mol^{-1}). INDO calculations[30] indicated that **Vb** is lower in energy than **Va** by 3 kcal mol^{-1}. However, we and others[2] anticipate that in most cases *CL*- and *AL*-$[V^{IV}O(sal\text{-}aa)(H_2O)]$ isomers in solution exist in similar concentrations.

When using characterisation in the solid state to explain observations in solution (*e.g.* by EPR), it is important to take into account that the observed solid-state structure may differ from that in solution. The solution or frozen solution EPR spectra for each of the $[V^{IV}O(sal\text{-}aa)(H_2O)]$ and $[V^{IV}O(sal\text{-}aa)(bpy)]$ complexes, or indeed most of the oxovanadium(IV) complexes with at least two non-equal adjacent equatorial donor atoms in a chelate molecule,[27] should correspond to mixtures of *endo* and *exo* diastereomers such as **Va** and **Vb**. For each isomer, geometric details affecting the electron donation of the donor groups and the π bonding established by each donor group will depend on its orientation relative to the vanadyl unit, as discussed previously for the imidazole ring.[31]

Optically active oxovanadium-(IV) or -(V) complexes, namely those with the N-salicylideneamino acidate ligands[2,32,33] have been used for several asymmetric transformations of organic compounds, *e.g.* enantioselective sulfide oxidations,[2,34] asymmetric epoxidations,[35] oxidative coupling of 2-naphthol,[20,32] Mukaiyama aldol additions and other reactions.[33] The V atom in most of the oxovanadium complexes used is a disymmetric centre and the relative concentration of the *C*- and *A*-complexes[28] certainly has an important role in the enantiomeric excesses obtained. However the relevance of this factor has never been previously addressed.

In order to achieve a better evaluation of the factors that determine the relative stabilities of diastereomers **Va** and **Vb** in $[V^{IV}O(sal\text{-}aa)(H_2O)]$ and $[V^{IV}O(sal\text{-}aa)(bpy)]$ complexes, and possible implications on some of their spectroscopic or catalytic properties, we also present here density functional and molecular mechanics calculations for several of these complexes.

Experimental

Preparations

$Na[V_2O_3(MeOsal\text{-}L\text{-}Ile)_2]\cdot H_2O$ **1**. The complex $[V^{IV}O(MeOsal\text{-}L\text{-}Ile)(H_2O)]$ **2** was prepared as described previously.[23] After precipitation of **2** from the reaction mixture, the solid was

Table 2 Crystal data and structure refinement for $Na[V_2O_3(MeOsal\text{-}L\text{-}Ile)_2]\cdot H_2O$ **1**

Empirical formula	$C_{28}H_{36}N_2NaO_{12}V_2$
Formula weight	717.46
Wavelength/Å	0.71073
Crystal system	Monoclinic
Space group	$P2_1$
a/Å	13.518(5)
b/Å	6.425(3)
c/Å	18.913(3)
β/°	106.523(2)
V/Å^3	1574.8(10)
Z	2
Absorption coefficient/mm^{-1}	0.672
F(000)	742
Reflections collected/unique	7851/3938 [*R*(int) = 0.0460]
Refinement method	Full-matrix least-squares on F^2
Data/restraints/parameters	3938/5/414
Final *R* indices [$I > 2\sigma(I)$]	$R_1 = 0.0487$, $wR_2 = 0.1048$

filtered off. The filtrate was kept at about 4 °C in a beaker covered with Parafilm®. After several months, dark crystals of **1** were separated and studied by X-ray diffraction.

Several [$V^{IV}O$(sal-aa)(H_2O)] and [$V^{IV}O$(sal-aa)(bpy)] complexes (aa = Ala, Val, Met; Phe, Ile and Leu) were prepared as described previously.[3,14,23]

EPR spectra

The X-band EPR spectra were recorded at 77 K either with a Bruker ESR-ER 200D connected to a Bruker B–MN C5 ESR spectrometer and to a Bruker ESR data system, or with a Brucker ESP 300 E spectrometer.

Circular dichroism and isotropic absorption spectra

CD spectra were run on a Jasco 720 spectropolarimeter with a red-sensitive (400–1000 nm) photomultiplier. UV/VIS absorption spectra were run with a Perkin Elmer L9 spectrophotometer.

Solid complex 1. The KBr disks for this purpose are prepared similarly to those for IR spectroscopy but (*i*) the relative amount of complex were *ca*. 50% higher, and (*ii*) the optical path was as low and homogeneous throughout the disk as possible. The disk was placed between two microscope slides and placed in the sample compartment in a fixed position. A first CD spectrum was run, the sample rotated ~70–90° and another spectrum recorded; five rotations were performed for the disk and the corresponding CD spectra recorded. With this type of solid sample, one does not know the position of the base line, but the correct pattern of the spectrum may be obtained if the CD signal recorded after each rotation of the sample is always approximately the same.

Crystallography

X-Ray diffraction measurements for **1** were made at room temperature on an Enraf-Nonius MACH3 diffractometer, using Mo-Kα radiation (λ(Mo-Kα) = 0.71073 Å). The crystal data and refinement details are given in Table 2. Using the CAD4 software, data were corrected for Lorentz and polarisation effects and empirically for absorption. The structure was solved with SHELXS-97[36] and refined by the full-matrix least-squares method with SHELXL97,[37] included in WinGX-Version 1.64.03B.[38]

Non-hydrogen atoms were anisotropically refined. The hydrogen atoms of all carbon atoms were inserted in calculated positions and refined isotropically, and the others were also refined isotropically riding with the parent carbon atom. The H atoms from the water molecule were found in the electron density map and allowed to refine isotropically with the O–H distances restrained to 1.00 Å. The illustrations were drawn with the programs ORTEP-II[39] included in OSCAIL Version 8[40] and SCHAKAL.[41] The atomic scattering factors and anomalous scattering terms were taken from ref. 42.

CCDC reference number 187826.

See http://www.rsc.org/suppdata/dt/b2/b205843j/ for crystallographic data in CIF or other electronic format.

Density functional calculations[43]

Full geometry optimisations were carried out on *C*- and *A*-[$V^{IV}O$(sal-L-Ala)(H_2O)] based on the X-ray structure of *C*-[$V^{IV}O$(sal-L-Ala)(H_2O)][5] and on a model compound of the mixed-valence complex **1**: $[V_2O_3(HOsal\text{-}Gly)_2]^-$ (HOsal-Gly = 4-hydroxysalicylideneglycinate), without symmetry constraints, using the Amsterdam Density Functional (ADF-2000) program[44] developed by Baerends and co-workers.[45] Vosko, Wilk and Nusair's local exchange correction potential was used,[46] together with Becke' nonlocal exchange[47] and Perdew's correlation corrections.[48] Unrestricted calculations with the gradient corrected geometry optimisation method[49] were performed. ADF basis set IV with frozen 1s, 2s, 2p shells was used for V, while basis set V was used for H and for C, N and O with 1s frozen cores. The ADF-2000 release was used to calculate the IR frequencies for *C*-[$V^{IV}O$(sal-L-Ala)(H_2O)] and the EPR parameters for the optimised geometry. All valence electrons were used for all atoms (type IV for V, type V for C, N, O, H). Relativistic effects were taken into account, within the "Zeroth Order Relativistic Approximation" ZORA formalism of ADF-2000.[44] The *g*-tensor calculations included spin–orbit coupling but were spin-restricted. In order to compare these results with other data available from the literature, similar calculations were performed on the complex $[VO(H_2O)_5]^{2+}$.

Molecular mechanics calculations

Molecular mechanics calculations were carried out using the Universal Force Field[50] within the CERIUS2 software.[51] The Universal force field is parameterised for the full periodic table. However the minimisation of the X-ray molecular structures of [$V^{IV}O$(sal-L-Ala)(H_2O)] and [$V^{IV}O$(sal-L-Ala)(bpy)] revealed clearly that the default values found in this force field were inappropriate to reproduce accurately the coordination spheres of this type of complexes. A specific set of parameters comprising the L–M bond lengths and L–M–L angles was developed empirically as described in the ESI.

Results and discussion

Crystallography

The solid complex $Na[V_2O_3(MeOsal\text{-}L\text{-}Ile)_2]\cdot H_2O$, **1**, was isolated from sodium acetate-containing solutions and its molecular structure is shown in Fig. 1. The formation of the mixed oxidation-state complex may be explained by the slow diffusion of atmospheric oxygen into the solution and reaction with oxovanadium(IV). In both half-units of **1** the configuration at the V atom is *C*.[27] The V(A)–O(6) and V(B)–O(6) are similar and the V–O–V angle is 170.9(3)°. Selected bond distances, angles as well as some of the relevant torsion angles are in Table 3. In the $V_2O_3^{3+}$ core the V=O bonds are *cis* to the bridge but *trans* to each other. For this type of arrangement the d_{xy} vanadium orbitals are nearly coplanar and are favourably oriented for an electronic interaction through the p_x orbital of the oxo bridge.[52,53]

The two V=O groups in complex **1** make an angle of 3.8°. Most bond lengths are similar in both half-units and comparable to those found in other N-salicylidene-aa complexes.[5,7] The water O7 is H-bonded with O2B and O2A of the molecule [O7–H7B ··· O2B 1.812(8) Å and [O7–H7A ··· O2A 1.838(8) Å]. Both O atoms of the vanadyl groups are H-bonded with a symmetry related molecule (x, $y + 1$, z) with distances 2.293(6)

Table 3 Selected bond lengths (Å), angles and torsion angles (°) for **1** (2nd and 5th columns) and for $[V_2O_3(HOsal\text{-}Gly)_2]^-$ (structure calculated by DFT—see text). Some data for relevent Na^+ ion distances are also included

VA–O(1A)	1.588(4)	1.604	O(1A)–VA–O(6)	108.4(3)	109.7
VA–O(6)	1.811(5)	1.775	O(1B)–VB–O(6)	107.8(3)	109.4
VA–O(4A)	1.868(4)	1.963	O(6)–VA–O(2A)	91.5(2)	92.9
VA–O(2A)	1.957(4)	1.965	O(6)–VB–O(2B)	88.9(2)	90.7
VA–N(1A)	2.090(5)	2.144	O(4A)–VA–O(2A)	145.9(2)	146.3
VB–O(1B)	1.581(4)	1.602	O(4B)–VB–O(2B)	146.8(2)	147.1
VB–O(6)	1.836(5)	1.790	O(6)–VA–N(1A)	149.9(2)	147.8
VB–O(4B)	1.886(4)	1.973	O(6)–VB–N(1B)	148.9(2)	146.9
VB–O(2B)	1.966(4)	1.971	O(1A)–VA–N(1A)	101.3(2)	102.5
VB–N(1B)	2.082(5)	2.134	O(1B)–VB–N(1B)	102.5(2)	103.5
N(1A)–C(3A)	1.286(7)	1.297	VA–O(6)–VB	170.9(3)	174.0
N(1A)–C(2A)	1.476(7)	1.459	O(1A)–VA–O(6)–VB	92(2)	96.0
O(4A)–C(5A)	1.320(7)	1.295	O(4A)–VA–O(6)–VB	−16(2)	−9.3
N(1B)–C(3B)	1.281(7)	1.298	O(2A)–VA–O(6)–VB	−162(2)	−155.8
N(1B)–C(2B)	1.478(6)	1.457	N(1A)–VA–O(6)–VB	−98(2)	−86
O(4B)–C(5B)	1.314(7)	1.295	O(1B)–VB–O(6)–VA	94(2)	86.7
C(2B)–C(10B)	1.545(7)	—	C(2A)–C(10A)	1.542(7)	—
Data for the Na^+ ion in **1**					
Na–O(3A)	2.349(5)	Na–O(7)#5	2.274(6)	Na–O(3B)#5	2.747(5)
Na–O(7)#4	2.245(6)	Na–O(3B)#6	2.388(5)	Na–Na#1	3.472(3)
				Na–Na#4	3.472(3)

Symmetry operations used: #1 $-x + 1, y - 1/2, -z$; #4 $-x + 1, y + 1/2, -z$; #5 $x, y + 1, z$; #6 $-x + 1, y + 3/2, -z$.

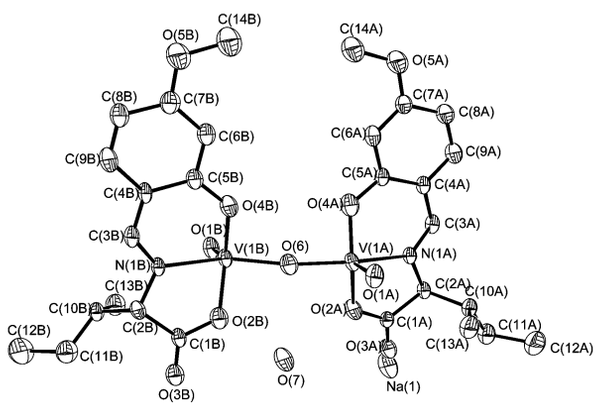

Fig. 1 An ORTEP diagram of $Na[V_2O_3(MeOsal\text{-}L\text{-}Ile)_2]\cdot H_2O$ **1** with thermal ellipsoids at 40% probability. H atoms were omitted for clarity. The atomic notation is indicated and similar numbering will be used throughout this work (*e.g.* C1, C2 and C10 for the carboxylate-, α- and β-carbon atoms of the amino acid, O1, O2, O4 and O5 for the vanadyl, carboxylate, phenolate and water O donor atoms, respectively). O6 is used for the bridging oxygen in dinuclear complexes.

Å (O1A ··· H3A–C3A), 2.222(7) Å (O1B ··· H3B–C3B), giving rise to dimerised packing of the dinuclear units along the *b* axis.

Each Na^+ is surrounded by five O atoms, O3B#5 at a longer distance (2.747(5) Å), in a distorted trigonal bipyramidal geometry, where two O3B atoms occupy the axial positions. The Na–O distances are listed in Table 3 and are comparable with those found in $Na[V_2O_3(sal\text{-}D,L\text{-}Ser)_2]\cdot 5H_2O$ [7] and hydrated sodium salts.[54] The oxygen coordination link together a line of Na^+ cations at a distance of 3.472(3) Å along the *b* direction.

DFT calculations

DFT calculations were performed both on a model of complex **1**: $[V_2O_3(HOsal\text{-}Gly)_2]^-$, and both *C*- and *A*-[V^{IV}O(sal-L-Ala)-(H_2O)] isomers, in order to understand several aspects of their structural preferences and electronic structure, and to determine some properties. The geometry of complex **1** was simplified by replacing the MeO group by HO in the benzene ring and the butyl chain by H. These substituents are located very far from the metal center and their effect is expected to be small

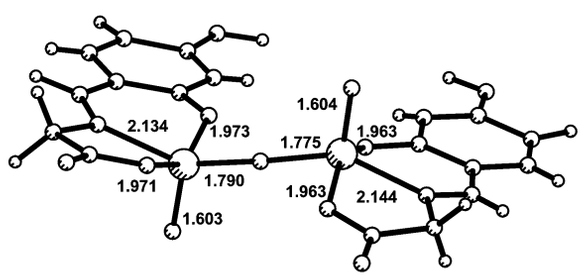

Fig. 2 DFT optimised structure of a model of complex **1**: $[V_2O_3(HOsal\text{-}Gly)_2]^-$, showing the distances in the vanadium coordination sphere (see text for details).

in most cases. The fully optimised structure is depicted in Fig. 2, and some bond lengths and angles are included in Table 3.

The calculated structural parameters compare well with those for **1**. Some of the differences arise from using an isolated molecule. For example, the V–O–V angle (174.0°) is closer to a linear disposition in $[V_2O_3(HOsal\text{-}Gly)_2]^-$. This effect may probably be ascribed to the presence of one water molecule near the bridging oxygen, H-bonded to both carboxylate (O2A and O2B) atoms, which may slightly distort the coordination environment of the metal. The calculated VA–($O_{carboxylate}$,$O_{phenolate}$,O_{water},N_{imine}) and VB–($O_{carboxylate}$,$O_{phenolate}$,O_{water},N_{imine}) bond lengths are close to those determined for **1**, almost within experimental error.

Complex **1**, formally containing V(v) and V(iv), can be described as a mixed valence complex. For the arrangement found in the $V_2O_3^{3+}$ core, it is expected that the spin density is extensively delocalised, and this is fully supported by the calculations. Indeed, in the model compound the spin density is distributed among the two V atoms (0.584 and 0.638), and the same small asymmetry found in the bond distances is observed here, since no symmetry constraints were taken in the calculations. The representation of the singly occupied SOMO is given in Fig. 3 and shows an extensive delocalization over the molecule.

DFT calculations were also done on the two diastereomers (**Va** and **Vb**), *endo*, *C*- and *exo*, *A*-[V^{IV}O(sal-L-Ala)(H_2O)], starting from the X-ray structure of *C*-[V^{IV}O(sal-L-Ala)(H_2O)]. Results from INDO calculations[30] are available (see Introduction) but they do not lead to the right energy ordering of the two isomers. However conformational energies are not expected

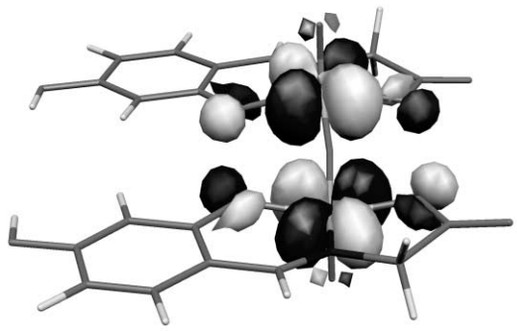

Fig. 3 Singly occupied SOMOs of a model of complex **1**: $[V_2O_3(HOsal\text{-}Gly)_2]^-$.

to be well described by semi-empirical methods. The V(IV) derivatives are paramagnetic species, so that spin unrestricted calculations are required (details in Experimental section). The *CL*- isomer (**Va**) was found to be more stable by 0.3 kcal mol^{-1}, in agreement with its presence in the crystal. However, such an energy difference may be fortuitous. The calculated structures of both complexes are shown in Fig. 4.

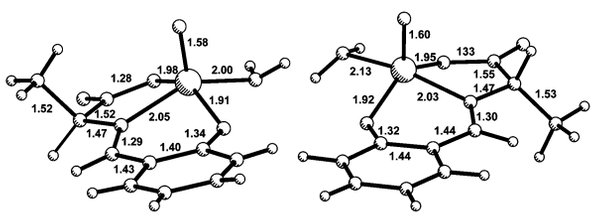

Fig. 4 DFT optimised structure of *C*- (left) and *A*-[$V^{IV}O$(sal-L-Ala)(H_2O)] (right), showing some relevant distances.

The bond distances do not vary much between the two isomers, the *CL*-isomer exhibiting shorter V=O and V–O (water and phenolate ring), but longer V–N and V–$O_{carboxylate}$ distances. These distances agree well with the experimental ones found in the X-ray crystal structure of *C*-[$V^{IV}O$(sal-L-Ala)(H_2O)].[5]

The singly occupied SOMO of both species is mainly located in the V atom (d_{xy} orbital), 85.5 and 83.9%, for *C*- and *A*-[$V^{IV}O$(sal-L-Ala)(H_2O)], respectively. The contribution of the vanadyl O atom to the SOMO is low (~0.7 and ~1.3%, respectively), as well as from the N_{imine} (~0.4 and ~0.3%, respectively), and from the equatorial H_2O (~0.6 and 0.9%, respectively). Besides the V atom, the most significant contributions are from the COO^- (~6 and 5%, respectively) and phenolate (~5 and ~7%, respectively) donor groups. These results support the traditional belief that in $V^{IV}O^{2+}$ compounds the unpaired electron is in a predominantly metal d_{xy} molecular orbital. The charge on the V atom was found to be about +1.45 (both isomers) and the spin density 1.14–1.15.

The analysis of the DFT-structures obtained for the *C*- and *A*-[$V^{IV}O$(sal-L-Ala)(H_2O)] diastereomers, particularly the torsion angles, show that the relative positions of the V=O/COO^-, V=O/N_{imine} are similar, those of V=O/$O_{phenolate}$ show small but significant differences. Therefore the spectroscopic properties expected for the two diastereomers, namely the donor-group contributions for $A_{||}$ and $g_{||}$, may present some, but not very pronounced, differences (see below).

DFT calculations were performed, for comparison, on the complex $[VO(H_2O)_5]^{2+}$, with only C_s symmetry, as when this work was started there were no *ab initio* calculations available. The charge on the V atom was found to be about 1.48 and the spin density 1.16. Table SM-5† summarises the structural data for $[VO(H_2O)_5]^{2+}$, including ESEM,[55–57] ENDOR[58] and X-ray measurements.[59] The DFT calculations agree well, as expected, with the recently reported DFT calculations also using the ADF program,[60] some differences resulting from the different symmetry assumed. Our DFT calculations also agree well with the X-ray diffraction data for $VO(H_2O)_5SO_4\beta$ (composed of isolated $[V^{IV}O(OH_2)_5^{2+}]$ units and isolated SO_4^{2+} tetrahedra).[59] Interestingly, for $[V^{IV}O(H_2O)_5]^{2+}$ the contribution of the V atom to the singly occupied SOMO is 88.5%, a higher value than that found for the alanine derivatives, owing to the better π-donor capabilities of the SB ligand compared to water. The SOMOs of the three oxovanadium(IV) complexes are shown in Fig. SM-4.† The π-donating properties of the SB ligand are well reflected in the antibonding V–O(phenolate, carboxylate) character of the SOMO of *C*-[$V^{IV}O$(sal-L-Ala)(H_2O)] and those of *AL*-[$V^{IV}O$(sal-L-Ala)(H_2O)].

Molecular mechanics calculations

Only the isomers in which the three donor atoms of the SB ligand occupy equatorial positions are considered in our MM calculations and entropic contributions, solvation, ion pairing, intermolecular H-bonding and electrostatic effects were not taken into account, as is often done for simple coordination compounds.[61] The strain energies of the isomers obviously depend on the force field parameterisation and other geometric restraints imposed, but the differences in the energy found between each two diastereomeric isomers **Va** and **Vb** gives a clear indication of their relative stability in the gas phase, and may be used to predict roughly their relative stability in solution. Indeed the optimised geometries compare well with those obtained in the DFT calculations and by X-ray diffraction, supporting the validity of the modelling procedures. The calculated bonding parameters are normal in as far as they lie within the range observed for other SB base complexes (see Table 1) with structure determined by X-ray diffraction. As an example the MM structures of *C*- and *A*-[$V^{IV}O$(sal-L-Ala)(bpy)] are shown in Fig. SM-1.†

For species of type [$V^{IV}O$(sal-L-aa)(H_2O)] the differences in the Δ*E*(*exo*/*endo*) (= *E*(*exo*) − *E*(*endo*)) are normally quite small (*ca.* ± 0.5–1 kcal mol^{-1}), being slightly larger for the L-Pen (L-Pen = L-2-amino-3-mercapto-3-methylbutanoic acid) and L-*tert*-butyl-Gly (−2.5 and −2.1 kcal mol^{-1}, respectively), indicating that in the gas phase isomers **Va** (*endo*) and **Vb** (*exo*) have similar stabilities (see Table SM-3†). However in the solid state the *endo* isomers are normally obtained (Table 1), possibly due to a more favourable packing. However, in solution studies both *endo* and *exo* isomers should be taken into account, and we anticipate that this applies to the great majority of oxovanadium complexes studied so far.

Some relevant molecular dimensions comprising intramolecular distances, angles and torsion angles are given in Table SM-4.† In the majority of MM minimised [$V^{IV}O$(sal-L-aa)(H_2O)] structures the SB ligand displays two planar parts (see Table SM-4†): one plane is defined by atoms C1, C2, O2 and O3, while O4, the aromatic carbon atoms and N1 and/or C3 determines the second plane. The angle between these two planes varies significantly with the amino acid and the diastereomer considered. However, the relative positions of the aromatic ring and chelate rings are approximately the same for all *CL*-isomers (*endo*) and all *AL*-isomers (*exo*), these relative positions differing between the *endo* and *exo* diastereomers.

For the six-coordinate [$V^{IV}O$(sal-L-aa)(bpy)] complexes the relative positions of the aromatic ring and the chelate rings exhibit similar relative positions for the *endo* and *exo* diastereomers. However, now the calculated energy differences Δ*E*(*exo*/*endo*) are always positive and in some cases significant (*e.g.* 2.2, 5.7, 6.4, 7.6 and 8.9 kcal mol^{-1} for aa = Phe, Val, Ile, Pen and *tert*-butyl-Gly, respectively). As for the [$V^{IV}O$(sal-L-aa)(H_2O)] complexes it is the degree of substitution at the β-carbon atom (C10) of the amino acid that is relevant, the following orders being observed for |Δ*E*(*exo*/*endo*)|: (i) Ala < Val ~Ile < 2-(*tert*-butylglycine), (ii) Cys ⩽ Pen. If only one extra group is

Table 4 Calculated (ADF-2000) and observed infrared wavenumbers for the *C*-[VO(sal-L-Ala)(H_2O)] complex[a]

Type of vibration	Calculated ν/cm^{-1} (intensity[b])	ν/cm^{-1} (KBr disk) (intensity[c])
*V=O stretching; C–H (CH_3) twisting and wagging; H_2O wagging	1028.7 (1.0)	996 (1.0)
C–O stretch (almost symmetric) H–C(=N) wagging; benzene-C–H wagging	1210.5 (1.189)	1127 (1.41), 1146 (1.39), 1208 (0.53)
*CH_3 and H–C(=N) twisting, α-C–H rocking; benzene-C–H twisting, C–$O_{phenolate}$ wagging	1329.1 (0.702)	1289 (0.82)
*Benzene-C–H twisting; CH_3 and H–C(=N) wagging	1560.0 (0.434)	1546 (0.85)
*C=N stretch; H–C(=N) out-of-plane bending, CH_3 and benzene-C–H twisting	1603.2 (2.097)	1599 (1.29)
* C=O stretch; H_2O and CH_3 wagging, H–C(=N) and benzene-C–H twisting	1720.8 (3.197)	1627 (1.38)
Antisymmetric OH stretch	3742.7 (0.655)	Broad band

[a] For almost all calculated wavenumbers all the molecule is involved in the vibration and the main group involved is mentioned first. If all molecule vibrates but one of the groups is more involved than others we include an asterisk for this group. [b] The intensities given are relative to the 1028.7 cm^{-1} band. The absorption intensity calculated for this band was 179.60 km mol^{-1}. [c] The intensities given are relative to the 996 cm^{-1} band, normally attributed to the stretching of the V=O, which may be considered as a strong band.

bonded to C10, *e.g.* –SH, –Ph, –$CH(CH_3)_2$, the bulkiness of this group is not particularly relevant. If the substitution is at the γ-carbon, as in Leu, rotation around the C2–C10 bond can occur more or less freely as several orientations of the amino acid side group lead to about the same strain energy.

In our MM calculations we found that the steric control favouring **Va** relative to **Vb** is determined by the non-bonded interactions between C10 and O3 ($O_{carboxylate}$), where the internuclear distances are often around 2.98–3.15 Å, *i.e.* below the sum of their *van der Waals radii* (Table SM-4†). The C10–C3 (C3 is the azomethine carbon) is occasionally also important. In addition in all MM structures the angle bending and torsion terms contribute significantly for the total steric energy, this often being greater than the *van der Waals* component.

As the V atom is normally above the "plane" of the four equatorial donor atoms,[27] in the *exo* isomers of six-coordinate complexes there is less space to accommodate the amino acid side group. For this reason, in the MM structures the amino acid side group tends to assume an "axial" arrangement in the *endo* isomer and "equatorial" orientation in the *exo* isomers, the typical values of the V–C2–C10 angles and torsion angles O1–V–C2–C10 reflect this fact (see Table SM-4†).

Infrared spectra

The IR spectrum for *C*-[V^{IV}O(sal-L-Ala)(H_2O)] was obtained from a frequency calculation with the ADF program, the wavenumbers, force constants and absorption intensities for IR bands being obtained. Table 4 (and SM-6) summarise the most intense bands in the calculated and experimental spectra, as well as the main groups involved in the vibrations. Some differences are expected between the calculated and experimental wavenumbers due to systematic errors in frequency calculations. Scaling factors are often applied to obtain better values.[62]

The ν(V=O) is obtained at 1028.7 cm^{-1} (see Fig. 5) as compared to the experimental 996 cm^{-1}. The C=N and $\nu_{as}(COO^-)$ stretches at 1603.2 and 1720.8 cm^{-1}, respectively, while the experimental are presumably at 1599 and 1627 cm^{-1}. Clearly the involvement of the COO^- group in H-bonding with neighbouring coordinated water molecules (C=O ··· H of 1.791 Å)[5] lowers its stretching frequency. The symmetric and antisymmetric O–H stretching of the coordinated water are calculated at 3610.3 and 3742.7 cm^{-1}, respectively. However, no individual sharp O–H stretching bands were identified in the experimental IR spectrum of polycrystalline samples of [V^{IV}O(sal-L-Ala)(H_2O)], but only a broad band (2600–3700 cm^{-1}) centred at ~3100 cm^{-1}. A medium/strong band at ~1530–1550 cm^{-1} typifies complexes derived from salicylaldehyde[14,23,63,64] and has been considered as originating from the vibration of (Ph)C–C(=N)[63] in the complexes. Two medium/strong bands were calculated for *C*-[V^{IV}O(sal-L-Ala)(H_2O)] in this wavenumber region, at 1529.4 and 1560.0 cm^{-1}, which involve the coupled vibrations of the benzene ring, the H–C(=N) group and C–O wagging, as well as of the coordinated water (scissoring) and carboxylate groups.

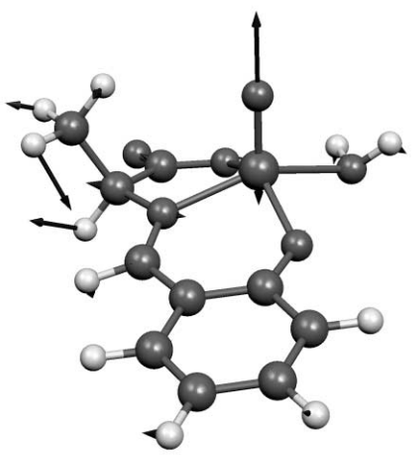

Fig. 5 Representation of the V=O stretching band in the complex *C*-[V^{IV}O(sal-L-Ala)(H_2O)] as obtained from a frequency calculation with the ADF-2000 program. This was calculated at 1028.7 cm^{-1} while the experimental ν(V=O) was found at 996 cm^{-1}.

The FT-IR of a polycrystalline sample of Na[V_2O_3(MeOsal-L-Ile)$_2$]·H_2O **1** is extremely complex. It presents a broad band (3700–3100 cm^{-1}) mainly due to ν(OH) centred at ~3350 cm^{-1}. The two medium-strong broad bands emerging at 3312 and 3270 cm^{-1} are probably due to the stretching of the H7A–O7–H7B water molecule (Fig. 1). In the FTIR of **1**, very strong bands appear at 1710, 1670 and ~1610 cm^{-1}, the latter is broad and has a shoulder in the lower wavenumber side due to overlap with aromatic ring-carbon stretching. In vanadium N-salicylideneamino acidate complexes, bands at 1620–1660 cm^{-1} and at 1590–1620 cm^{-1} have been attributed to ν(C=N) and $\nu_{as}(COO^-)$, respectively. However, taking into account the results obtained by the ADF program we conclude that these bands should be ascribed to $\nu_{as}(COO^-)$ and ν(C=N), respectively.

The region 1200–1450 cm^{-1} is confusingly crowded with strong and mostly sharp bands. The IR of L-isoleucine is also very complex in this region, and this should be partly due to aliphatic C–H deformation bands. Based on the calculated ν_s(COO) for *C*-[V^{IV}O(sal-L-Ala)(H_2O)] (Table 4) at 1210 cm^{-1}, we ascribe the symmetric carboxylate stretch of **1** to one (or both) of the medium/strong bands at 1212 and 1231 cm^{-1}. Medium to strong bands in the range 1270 and 1330 cm^{-1} have been ascribed to ν(O–Ph). There are four strong bands in the 1270–1330 cm^{-1} range in the IR of **1**. Based on the calculated value for *C*-[V^{IV}O(sal-L-Ala)(H_2O)]: 1329.1 cm^{-1} (this is a complex vibration that includes O–Ph, Table 4), we ascribe the ν(O–Ph) of **1** to the strong band at 1300 cm^{-1}. The ν(V=O) band appears at 978 cm^{-1}, with a shoulder on the lower wavenumber

Table 5 EPR parameters obtained from the experimental EPR spectra[67] and back-calculated $A_{||}$(imine) values for each complex and $(\beta^*)^2$[a]

aa in VO(sal-L-aa)	$g_{||}$	$A_{||} \times 10^4/cm^{-1}$	Back-calculated $A_{||}$(imine) $\times 10^4/cm^{-1}$	$g_\perp$ ($A_\perp \times 10^4/cm^{-1}$)	$(\beta^*)^2$
$V^{IV}O$(sal-L-aa)(H_2O) complexes					
Ala	1.938	164.5	37.88	1.982 (62.0)	0.853
Val	1.949	163.5	36.88	1.984 (63.2)	0.846
Met	1.949	164.5	37.88	1.982 (62.8)	0.859
Phe	1.944	163.0	36.38	1.982 (63.0)	0.838
Ile	1.939	163.9	37.28	1.980 (63.2)	0.839
Leu	1.941	164.1	37.48	1.981 (63.0)	0.845
Cys	1.933	164.8	38.18	1.977 (62.8)	0.845
$V^{IV}O$(sal-L-aa)(bpy) complexes					
Ala	1.952	159.6	37.92	1.988 (61.6)	0.826
Val	1.952	159.1	37.38	1.983 (58.9)	0.848
Met	1.950	158.3	36.66	1.984 (59.1)	0.837
Phe	1.952	158.4	36.70	1.984 (59.0)	0.841
Cys	1.942	161.2	39.52	1.977 (59.2)	0.855
S-Me-Cys	1.950	162.0	40.32	1.981 (58.5)	0.877
S-Et-Cys	1.951	162.1	40.42	1.981 (58.2)	0.881
D-Pen	1.935	159.7	38.02	1.974 (58.2)	0.844

[a] The square of the orbital coeficent, $(\beta^*)^2$, may be obtained from the equation:[68,69] $(\beta^*)^2 = 7/6[(A_{||} - A_\perp)/P - \Delta g_{||} + 5/14\Delta g_\perp)]$, with $\Delta g_{||} = 2.0023 - g_{||}$ and $\Delta g_\perp = 2.0023 - g_\perp$, taking $P = 0.0130\ cm^{-1}$. The quantity $(\beta^*)^2$ corresponds to the coefficient of the vanadium $3d_{xy}$ orbital in the SOMO molecular orbital.

side. The appearance of two bands may result from the non-equivalence of the two V=O groups of **1**, partly due to their involvement in distinct types of H-bonds.

CD spectra of 1

The CD spectrum of a KBr disk of **1** in the 400–1000 nm range shows four distinct bands at 465 ($\Delta A > 0$), 560 ($\Delta A > 0$), 725 ($\Delta A < 0$) and 890 nm ($\Delta A > 0$). The two low energy bands correspond to band I ($d_{xy} \longrightarrow d_{xz}$ and $d_{xy} \longrightarrow d_{yz}$), emphasising the non-symmetrical nature of the ligand field. The band at 560 nm may be assigned to band II ($d_{xy} \longrightarrow d_{x^2-y^2}$).[14,27] Upon dissolving in water the pattern of the CD spectrum changes presenting bands at ~440 ($\Delta A > 0$), 535 ($\Delta A < 0$), 735 ($\Delta A > 0$) and 950 nm ($\Delta A < 0$), a pattern similar to the CD spectrum of [VO(sal-L-Ile)(H_2O)] in methanol.[14] These results indicate that the binding mode around vanadium changes upon dissolving **1** in water, where the CD signal is then mainly due to [VO(MeOsal-L-Ile)(H_2O)].

EPR spectra

The structure of **1** determined by X-ray diffraction corresponds to an *anti*-orthogonal arrangement of the $V_2O_3^{3+}$ core and, as mentioned above, this configuration allows effective delocalization of the electron over both vanadium ions as was observed in other similar mixed-valence complexes, *e.g.* $[V_2O_3(nta)_2]^{3-}$,[52] $[V_2O_3(pmida)_2]^{-}$[53] and $[V_2O_3(sal\text{-}L\text{-}Ala)_2]^{-}$,[16] where the very strong intramolecular antiferromagnetic coupling is expected to proceed *via* this superexchange pathway.[65,66] The X-band EPR spectrum of a powdered sample of **1** gave a broad signal centred at $g = 1.986$ (300 and 77 K), similar to those of oxovanadium(IV) complexes. At room temperature no EPR signal could be measured for **1** in water but at 77 K the signal shows broad structured bands. Upon addition of ethylene glycol the signal ($g_{||}$, $g_\perp$, $A_{||}$, $A_\perp$ = 1.949, 1.978, 168, 60.8 $\times 10^{-4}$ cm^{-1}, respectively) is similar to those of monomeric $[V^{IV}O$(sal-aa)-(H_2O)] complexes, indicating that **1** decomposed upon dissolution in water. This is consistent with the CD measurements (see above).

The EPR parameters obtained for $[V^{IV}O$(sal-aa)(H_2O)] and $[V^{IV}O$(sal-aa)(bpy)] complexes in methanol are in Table 5. These were obtained by spectral simulation[67] of the experimental frozen (77 K) solution spectra. This Table also includes the unpaired ground state (d_{xy}) orbital population $(\beta^*)^2$ estimated from the EPR spectra. These values are similar to those obtained by DFT for *C*- and *A*-$[V^{IV}O$(sal-L-Ala)(H_2O)], and indicate that the unpaired electron is mostly localised in the d_{xy} orbital.

The EPR parameters were also obtained for *A*- and *C*-$[V^{IV}O$(sal-L-Ala)(H_2O)] complexes in DFT spin restricted calculations including relativistic and spin–orbit coupling corrections. The calculated *g* and *A* parameters differ for the two diastereomers but the differences are rather unimportant (Table 6). This means that in this case the difference in molecular structures is not significantly reflected on the calculated EPR spectra, as expected, since the structural differences do not involve the coordination sphere of vanadium, but take place at the periphery. The DFT-calculated g_x, g_y, g_z for *A*- and *C*-$[V^{IV}O$(sal-L-Ala)(H_2O)] agree well with the experimental $g_\perp$ and $g_{||}$ values (Table 6), but the same does not apply for the hyperfine coupling constants. The EPR parameters of $[V^{IV}O(H_2O)_5]^{2+}$ were calculated in the same conditions for calibration (Table 6). Again the agreement between calculated and experimental hyperfine coupling constants is not very good. In fact the recently reported DFT calculations for $[V^{IV}O(H_2O)_5]^{2+}$ also yielded systematically too low *A* values but reasonably good *g* values.[55] Constraints in the calculations, such as the functionals used,[71] spin restrictions, accounting for spin–orbit effects, may be reponsible for the deviations between calculated and experimental values.

It is well known that the EPR spectra may help to elucidate which groups coordinate in equatorial position in solution and for this purpose the so-called additivity relation[72] is often used. Back-calculation of the N_{imine} contribution gives an average of 37.3 and 38.2 $\times 10^{-4}$ cm^{-1} for the $A_{||}$ values of the $[V^{IV}O$-(sal-aa)(H_2O)] and $[V^{IV}O$(sal-aa)(bpy)] complexes, respectively. These values are among the lowest for aromatic imine donors,[31] but are close to the $A_{||}(R–O^-)$ and higher than those for $N_{peptide}$ (35–36 $\times 10^{-4}$ cm^{-1}).[73,74] Low $A_{||i}$ (i represents the donor groups coordinated equatorially) contributions reflect a reduced electron-nuclear hyperfine interaction resulting from a reduced effective charge on the metal and some delocalization of unpaired spin density onto the ligands.

Cornman *et al.*[75] discussed the decrease in the total $A_{||}$ values of ligands containing phenolate and imine donors as resulting from the distortion towards a trigonal bipyramidal geometry. Smith *et al.*[31] demonstrated that the contribution of the $N_{imidazole}$ depends on the relative orientation of the imidazole ring and the V=O group, this determining the degree of overlap between the $N_{imidazole}$ aromatic p orbital and the d_{xy} vanadium

Table 6 EPR parameters calculated by the ADF-2000 for the *C*- and *A*-[$V^{IV}O$(sal-L-Ala)(H_2O)], and the [$V^{IV}O(H_2O)_5^{2+}$] complexes

	CL-diastereomer	*AL*-diastereomer	[$V^{IV}O(H_2O)_5^{2+}$] (C_s symmetry)	[$V^{IV}O(H_2O)_5^{2+}$][60] (C_{2v} symmetry)
EPR Parameters[a]				
g_z, $\|A_z\|$	1.9387, 49.9	1.9318, 48.5	1.902, 57.7	1.930, 136
g_x, g_y	1.9866, 1.9817	1.9872, 1.9829	1.968, 1.641	1.986, 1.986
$\|A_x\|$, $\|A_y\|$	20.7, 17.5	19.5, 17.7	19.5, 19.1	49, 49
Experimental[a]	VO(sal-L-Ala)(H_2O)[9]		[$V^{IV}O(H_2O)_5^{2+}$][70]	
g_z, $\|A_z\|$	1.938, 164.5		1.932, 182.6	
g_x, g_y	1.982		1.980	
$\|A_x\|$, $\|A_y\|$	62		71.3	

[a] Hyperfine coupling constants are multiplied by 10^{-4} cm^{-1}.

orbital. For the *C*- and *A*-[$V^{IV}O$(sal-L-Ala)(H_2O or bpy)] complexes the degree of distortion from a square-pyramidal geometry is about the same for the *CL*- and *AL*-diastereomers. On the other hand, the torsion angles defining the relative positions of the donor atoms of the SB ligand and the vanadyl unit show characteristic patterns for the *CL* or *AL* isomers, Table SM-4†, showing that while the torsion angles O1–V–**O4**–C5 and O1–V–**N1**–C2 are always positive for the *CL*- and negative for the *AL*-diastereomers, those of O1–V–**O2**–C1 and O1–V–**N1**–C3 are always negative for the *CL*- and positive for the *AL*-diastereomers. However, the possibility of each donor group, namely the $O_{phenolate}$, to establish π bonds with vanadium d orbitals, particularly the d_{xy} orbital, differs for the *CL*- and *AL*-diastereomers, but not very significantly. This was also confirmed in our DFT results for the *C*- and *A*-[$V^{IV}O$(sal-L-Ala)(H_2O)] diastereomers, where the contributions of the $O_{phenolate}$ to the SOMO orbital were found to be ~5 and ~7%, respectively.

Once some stereochemical characteristics differ, one could expect that the two diastereomers should have some distinct spectroscopic properties, *e.g.* the Cotton effects and contributions of $O_{phenolate}$ to the hyperfine coupling constant. As far as the hyperfine coupling constants are concerned, the experimental observation is that the $A_{||}$ values are all within 163.8 ± 1 × 10^{-4} cm^{-1} for the [$V^{IV}O$(sal-aa)(H_2O)] complexes and 160.1 ± 2.0 × 10^{-4} cm^{-1} for the [$V^{IV}O$(sal-aa)(bpy)] compounds, and the back-calculated N_{imine} contributions are almost all within 38.5 ± 1.5 × 10^{-4} cm^{-1}. Therefore, the overall effect is such that the measured $A_{||}$ values are about the same in all isomers, and this probably results from the low participation of the $O_{phenolate}$, $O_{carboxylate}$ and N_{imine} in the SOMO molecular orbital containing the unpaired electron.

Chirality in transition metal compounds, and particularly in amino acid complexes, is generally attributed to specific structural features discussed elsewhere.[76,77] It was observed previously for the [$V^{IV}O$(sal-aa)(H_2O)] complexes that the Cotton effect in the 300–1000 nm range increases with the bulkiness of the amino acid side-group.[14] However, this trend is not related to the relative amount of the *CL*- and *AL*-diastereomers found here. Therefore, our results indicate that, for the present systems, the rotatory strengths are determined by the vicinal dissymetry effect and not by the inherent dissymetry effect.[76,77]

Conclusions

The dinuclear complex: Na[V_2O_3(MeOsal-L-Ile)$_2$]·H_2O **1** was prepared and characterised by X-ray diffraction. It consists of two VO(MeOsal-L-Ile) units and its molecular structure is similar to several of the mixed valence complexes containing the $V_2O_3^{3+}$ core previously reported. The V^{IV}–O–V^{V} bridge is almost linear, indicating extensive delocalization of the unpaired electron. The structure of [V_2O_3(HOsal-L-Gly)$_2$]$^-$ was calculated by DFT methods and compares well with the structure of **1**. In this model compound the spin density is distributed among the two V atoms, confirming extensive delocalization over the molecule, particularly through the d_{xy} orbitals of both V atoms.

Molecular mechanics and DFT methods were used to calculate the structures and the main factors that determine the relative energies of the *CL*- and *AL*-[$V^{IV}O$(sal-aa)(X)] diastereomeric complexes (X = H_2O or bpy). The results obtained indicate that for X = bpy, at least in the gas phase the *CL*-diastereomers are more stable than the *AL*-diastereomers, the energy difference increasing with the degree of substitution on the β-carbon atom of the amino acid. When X = H_2O the *CL*- and *AL*-diastereomers correspond to about the same energies. This indicates that when using oxovanadium complexes for asymmetric transformations of organic molecules, *e.g.* enantioselective sulfide oxidations, epoxidations or other reactions where the enantioselectivity might be induced by the optically active oxovanadium complexes, the relative concentration of the *C* and *A* isomeric complexes[28] should be taken into account, and if possible evaluated. If in the active complex one of the configurations *C* or *A* is not predominant, low enantiomeric excesses will probably be obtained.

DFT methods were also used to calculate the IR spectrum of *C*-[$V^{IV}O$(sal-L-Ala)(H_2O)] which compared well with the experimental. The implications of the presence of both *C*- and *A*-[$V^{IV}O$(sal-*L*-aa)(H_2O)] diastereomers in the g_z and A_z EPR parameters were discussed, the overall conclusion being that no significant differences are to be expected.

Acknowledgements

The authors are grateful to the Fundo Europeu para o Desenvolvimento Regional, Fundação para a Ciência e Tecnologia and the POCTI Programme (project POCTI/35368/QUI/2000).

References

1 J. J. R. Fraústo da Silva, R. Wootton and R. D. Gillard, *J. Chem. Soc. A*, 1970, 3369–3372.
2 K. Nakajima, M. Kojima, K. Toriumi, K. Saito and J. Fujita, *Bull. Chem. Soc. Jpn.*, 1989, **62**, 760–767.
3 L. J. Theriot, G. O. Carlisle and H. J. Hu, *J. Inorg. Nucl. Chem.*, 1969, **31**, 2841–2844.
4 A. Syamal and L. J. Theriot, *J. Coord. Chem.*, 1973, **2**, 193–200.
5 R. Hämäläinen and U. Turpeinen, *Acta Crystallogr., Sect. C*, 1985, **41**, 1726–1728.
6 L. Casella, M. Gullotti, A. Pintar, S. Colonna and A. Manfredi, *Inorg. Chim. Acta*, 1988, **144**, 89–97.
7 J. Costa Pessoa, J. A. L. Silva, A. L. Vieira, L. Vilas Boas, P. O'Brien and P. Thornton, *J. Chem. Soc., Dalton Trans.*, 1992, 1745–1749.
8 V. Vergopoulos, W. Priebsch, M. Fritzsche and D. Rehder, *Inorg. Chem.*, 1993, **32**, 1844–1849.
9 I. Cavaco, J. Costa Pessoa, D. Costa, M. T. Duarte, R. D. Gilard and P. Matias, *J. Chem. Soc., Dalton Trans.*, 1994, 149–157.
10 I. Cavaco, J. Costa Pessoa, S. M. Luz, M. T. Duarte, P. M. Matias, R. T. Henriques and R. D. Gillard, *Polyhedron*, 1995, **14**, 429–439.
11 S. Dutta, S. Mondal and A. Chakravorty, *Polyhedron*, 1995, **14**, 1163–1168.
12 S. Mondal, S. Dutta and A. Chakravorty, *J. Chem. Soc., Dalton Trans.*, 1995, 1115–1120.

13 R. Fulwood, H. Schmidt and D. Rehder, *J. Chem. Soc., Chem. Commun.*, 1995, 1443–1444.
14 I. Cavaco, J. Costa Pessoa, M. T. Duarte, R. T. Henriques, P. M. Matias and R. D. Gillard, *J. Chem. Soc., Dalton Trans.*, 1996, 1989–1996.
15 I. Cavaco, J. Costa Pessoa, M. T. L. Duarte, P. M. Matias and R. D. Gillard, *Chem. Commun.*, 1996, 1365–1366.
16 S. Mondal, P. Ghosh and A. Chakravorty, *Inorg. Chem.*, 1997, **36**, 59–63.
17 K. K. Rajak, S. S. Rath, S. Mondal and A. Chakravorty, *J. Chem. Soc., Dalton Trans.*, 1999, 2537–2540.
18 S. Mondal, S. S. Rath, K. K. Rajak and A. Chakravorty, *Inorg. Chem.*, 1998, **37**, 1713–1719.
19 K. K. Rajak, S. S. Rath, S. Mondal and A. Chakravorty, *Inorg. Chem.*, 1999, **38**, 3283–3289.
20 S. W. Hon, C. H. Li, J. H. Kuo, N. B. Barhate, Y. H. Liu, Y. Wang and C. T. Chen, *Org. Lett.*, 2001, **3**, 869–872.
21 W. Chen, S. Gao and A. X. Liu, *Acta Crystallogr., Sect. C*, 1999, **55**, 531.
22 J. Costa Pessoa, M. T. Duarte, R. D. Gillard, C. Madeira, P. M. Matias and I. Tomaz, *J. Chem. Soc., Dalton Trans.*, 1998, 4015–4020.
23 J. Costa Pessoa, I. Cavaco, I. Correia, M. T. Duarte, R. D. Gillard, R. T. Henriques, F. J. Higes, C. Madeira and I. Tomaz, *Inorg. Chim. Acta*, 1999, **293**, 1–11.
24 C. Grüning, H. Schmidt and D. Rehder, *Inorg. Chem. Commun.*, 1999, **2**, 57–59.
25 J. Costa Pessoa, I. Cavaco, I. Correia, D. Costa, R. T. Henriques and R. D. Gillard, *Inorg. Chim. Acta*, 2000, **305**, 7–13.
26 S. Mondal, S. P. Rath, S. Dutta and A. Chakravorty, *J. Chem. Soc., Dalton Trans.*, 1996, 99–103.
27 L. F. Vilas Boas and J. Costa Pessoa, in *Comprehensive Coordination Chemistry*, ed. G. Wilkinson, R. D. Gillard and J. A. McCleverty, Pergamon, Oxford, 1987, vol. 3, pp. 453–583.
28 G. J. Leigh, in *Nomenclature of Inorganic Chemistry*, ed. G. J. Leigh, Blackwell, Oxford, 1990, p. 186.
29 T. R. Cundari, L. L. Sisterhen and C. L. Stylianopoulos, *Inorg. Chem.*, 1997, **36**, 4029.
30 T. R. Cundari, L. Saunders and C. L. Stylianopoulos, *J. Phys. Chem. A*, 1998, **102**, 997–1004.
31 T. S. Smith, C. A. Root, J. W. Kampf, P. G. Rasmussen and V. L. Pecoraro, *J. Am. Chem. Soc.*, 2000, **122**, 767–775 and references therein.
32 S. W. Hon, N. B. Barhate, J. H. Kuo, C. H. Li and C. T. Chen, poster at the 3rd International Symposium on Chemistry and Biological Chemistry of Vanadium, P-78, Osaka, November, 2001; C. Y. Chu and B. J. Uang, poster at the 3rd International Symposium on Chemistry and Biological Chemistry of Vanadium, P-79, Osaka, November, 2001.
33 S. W. Hon, N. B. Barhate, J. H. Kuo, C. H. Li and C. T. Chen, poster at the 3rd International Symposium on Chemistry and Biological Chemistry of Vanadium, P-70, Osaka, November, 2001.
34 (*a*) K. Nakajima, K. Kojima, M. Kojima and J. Fujita, *Bull. Chem. Soc. Jpn.*, 1990, **63**, 2620–2630; (*b*) H. Schmidt, M. Bashirpoor and D. Rehder, *J. Chem. Soc., Dalton Trans.*, 1996, 3865–3870 and refs. therein; (*c*) C. Bolm and F. Bienewald, *Angew. Chem., Int. Ed. Engl.*, 1995, **34**, 2640; (*d*) C. Bolm and F. Bienewald, *Synlett*, 1998, 1327.
35 C. Bolm and T. Kühn, *Synlett*, 2000, 899; C. Bolm, presented at the 3rd International Symposium on Chemistry and Biological Chemistry of Vanadium, I-3, Osaka, November, 2001.
36 SHELXS-97: G. M. Sheldrick, *Acta Crystallogr., Sect. A*, 1990, **46**, 467–473.
37 SHELXL-97 : G. M. Sheldrick, *A computer program for refinement of crystal structures*, University of Göttingen, 1997.
38 L. J. Farrugia, Oscail Version 8, *J. Appl. Crystallogr.*, 1999, **32**, 837–838.
39 E. Keller, SCHAKAL 99, *Graphical representation of molecular models*, University of Freiburg, Germany, 1999.
40 P. McArdle, Oscail Version 8, *J. Appl. Crystallogr.*, 1995, **28**, 65–65.
41 M. N. Burnett and C. K. Johnson, ORTEP III: Oak Ridge Thermal Ellipsoid Plot Program for Crystal Structure Illustrations, Oak Ridge National Laboratory Report ORNL-6895, Oak Ridge National Laboratory, TN, 1996.
42 *International Tables for X-Ray Crystallography*, Kynoch Press, Birmingham, UK, 1974, vol. IV.
43 R. G. Parr and W. Yang, *Density Functional Theory of Atoms and Molecules*, Oxford University Press, New York, 1989.
44 (*a*) ADF (2000): E. J. Baerends, A. Bérces, C. Bo, P. M. Boerrigter, L. Cavallo, L. Deng, R. M. Dickson, D. E. Ellis, L. Fan, T. H. Fischer, C. Fonseca Guerra, S. J. A. van Gisbergen, J. A. Groeneveld, O. V. Gritsenko, F. E. Harris, P. van den Hoek, H. Jacobsen, G. van Kessel, F. Kootstra, E. van Lenthe, V. P. Osinga, P. H. T. Philipsen, D. Post, C. C. Pye, W. Ravenek, P. Ros, P. R. T. Schipper, G. Schreckenbach, J. G. Snijders, M. Sola, D. Swerhone, G. te Velde, P. Vernooijs, L. Versluis, O. Visser, E. van Wezenbeek, G. Wiesenekker, S. K. Wolff, T. K. Woo and T. Ziegler; (*b*) C. Fonseca Guerra, O. Visser, J. G. Snijders, G. te Velde and E. J. Baerends, Parallelisation of the Amsterdam Density Functional Programme, in *Methods and Techniques for Computational Chemistry*, ed. E. Clementi and C. Corongiu,STEF, Cagliari, 1995, pp. 303–395; (*c*) C. Fonseca Guerra, J. G. Snijders, G. te Velde and E. J. Baerends, *Theor. Chem. Acc.*, 1998, **99**, 391.
45 (*a*) E. J. Baerends, D. Ellis and P. Ros, *Chem. Phys.*, 1973, **2**, 41; (*b*) E. J. Baerends and P. Ros, *Int. J. Quantum Chem.*, 1978, **S12**, 169; (*c*) P. M. Boerrigter, G. te Velde and E. J. Baerends, *Int. J. Quantum Chem.*, 1988, **33**, 87; (*d*) G. te Velde and E. J. Baerends, *J. Comput. Phys.*, 1992, **99**, 84.
46 S. H. Vosko, L. Wilk and M. Nusair, *Can. J. Phys.*, 1980, **58**, 1200.
47 A. D. Becke, *J. Chem. Phys.*, 1987, **88**, 1053.
48 (*a*) J. P. Perdew, *Phys. Rev. B*, 1986, **33**, 8822; (*b*) J. P. Perdew, *Phys. Rev. B*, 1986, **34**, 7406.
49 (*a*) L. Versluis and T. Ziegler, *J. Chem. Phys.*, 1988, **88**, 322; (*b*) L. Fan and T. Ziegler, *J. Chem. Phys.*, 1991, **95**, 7401.
50 A. K. Rappé, C. J. Casewit, K. S. Colwell, W. A. Goddard III and W. M. Skiff, *J. Am. Chem. Soc.*, 1992, **114**, 10024.
51 CERIUS 2, version 3.5, Molecular Simulations Inc., San Diego, 1997.
52 M. Nishizawa, K. Hirotsu, S. Ooi and K. Saito, *J. Chem. Soc., Chem. Commun.*, 1979, 707.
53 J. P. Launay, Y. Jeannin and M. Daoudi, *Inorg. Chem.*, 1985, **24**, 1052.
54 (*a*) J. Burgess, Ions in Solution: *Basic Principles of Chemical Interactions*, Halsted Press, New York, 1988, p. 40; (*b*) D. E. Fenton, in *Comprehensive Coordination Chemistry*, ed. G. Wilkinson, R. D. Gillard and J. A. McCleverty, vol. 3, Pergamon, Oxford, 1987, pp. 4–6.
55 L. Kevan, *J. Phys. Chem.*, 1984, **88**, 327–328.
56 D. Suryanarayana, P. A. Narayana and L. Kevan, *J. Phys. Chem.*, 1982, **86**, 4579.
57 S. A. Dikanov, V. F. Yudanov and Yu. D. Tsvetkov, *J. Magn. Reson.*, 1979, **34**, 631.
58 N. M. Atherton and J. F. Shackelton, *Mol. Phys.*, 1980, **39**, 1471.
59 M. Tachez and F. Theobald, *Acta Crystallogr., Sect. B*, 1980, **36**, 1757–1761.
60 (*a*) P. J. Carl, S. L. Isley and S. C. Larsen, *J. Phys. Chem. A*, 2001, **105**, 4563–73; (*b*) S. C. Larsen, *J. Phys. Chem. A*, 2001, **105**, 8333–8338.
61 (*a*) P. Comba, *Coord. Chem. Rev.*, 1999, **182**, 343–371; (*b*) P. Comba and T. W. Hambley, *Molecular Modelling of Inorganic Compounds*, Wiley-VCH, Weinheim, 1995.
62 J. B. Foresman and A. Frisch, *Exploring Chemistry with Electronic Structure Methods*, Gaussian Inc., Pittsburgh, PA, 1996.
63 J. W. Leadbetter and Jun, *J. Phys. Chem.*, 1977, **81**, 54.
64 L. Casella and M. Gullotti, *J. Am. Chem. Soc.*, 1981, **103**, 6338.
65 D. Schulz, T. Weyhermüller, K. Wieghardt and B. Nuber, *Inorg. Chim. Acta*, 1995, **240**, 217–229.
66 H. Toftlund, S. Larsen and K. S. Murray, *Inorg. Chem.*, 1991, **30**, 3964.
67 EPRPOW, developed by L. K. White, R. L. Belford (University of Illinois) and modified by L. K. White, N. F. Albanese and N. D. Chasteen (University of New Hampshire) to include both Lorentzian and Gaussian line shape functions, an $I = 7/2$ nucleus, a 4th hyperfine interaction and multiple sites having different linewidths, 1978.
68 K. P. Callahan and P. J. Durand, *Inorg. Chem.*, 1980, **19**, 3214.
69 B. N. Figgis and M. A. Hitchman, *Ligand Field Theory and its Applications*, Wiley-VCH, New York, 2000, pp. 294–303.
70 R. H. Borcherts and K. Kikushi, *J. Chem. Phys.*, 1964, **41**, 1596.
71 F. Neese, *J. Inorg. Biochem.*, 2001, **86**, 357.
72 N. D. Chasteen, in *Biological Magnetic Resonance*, ed. L. J. Berliner, J. Reuben, Plenum, New York, 1981, vol. 3, p. 53.
73 A. J. Tasiopoulos, E. J. Tolis, J. M. Tsangaris, A. Evangelou, J. D. Woollins, A. M. Z. Slawin, J. Costa Pessoa, I. Correia and T. A. Kabanos, *J. Biol. Inorg. Chem.*, 2002, **7**, 363–374.
74 J. Costa Pessoa, S. M. Luz and R. D. Gillard, *J. Chem. Soc., Dalton Trans.*, 1997, 569.
75 C. R. Cornmann, K. M. Geiser-Bush, S. P. Rowley and P. D. Boyle, *Inorg. Chem.*, 1997, **36**, 6401–6408.
76 F. S. Richardson, *Chem. Rev.*, 1979, **79**, 17–35.
77 R. Kuroda and Y. Saito, in *Circular Dichroism: principles and applications*, ed. K. Nakanishi, N. Berova and R. W. Woody, VCH, New York, 1994, pp. 223–225.